ISSN 2541-223X
Volume 4 2022

SEISMIC LOAD REDUCTION ON THE BRIDGE OVER LIQUEFACTION VULNERABILITY ZONE BY LEAD RUBBER BEARING

A Zakariya[1], A Rifa'i[1,*], S Ismanti[1]

[1]Department of Civil and Environmental Engineering, Universitas Gadjah Mada, Sleman, Indonesia, 55281

ABSTRACT

The Palu IV bridge collapsed after the 2018 Palu earthquake. Bridge failure is caused by moment force and buckling increasing simultaneously while liquefaction occurs. This study performs a simulation of the Kretek 2 Bridge by three models; pinned and roller support, bearing pad, and lead rubber bearing to understand seismic load reduction with different supports. The bridge load refers to SNI 1725:2016 and SNI 2833:2016. Site-specific response spectra are required due to near earthquake sources. The analysis result using MIDAS both bearing pads and lead rubber bearings show a significant reduction in beam forces. Axial forces, shear Y, shear Z, moment Y and moment Z, for bearing pad model were reduced to -10.79%, -7.28%, -74.59%, -65.51%, and -19.28%, respectively, whereas for lead rubber bearings model were reduced to -10.88%, +5.29%, -72.75%, -63.48%, and -7.34% respectively. However, the displacement in the bearing pad reaches 0.221m exceeding a boundary maximum of 0.050mm, so it cannot be used. Displacement of lead rubber bearing reaches 0.162m, which is still below 0.384mm. Thus, a lead rubber bearing used as a seismic isolation damper is appropriate for the Kretek 2 Bridge.

Keywords: bridge failure, bearing pad, lead rubber bearing, MIDAS, beam forces, displacement

1. INTRODUCTION

The Palu earthquake occurrence in 2018 resulted in severe damage to many infrastructures, one of which was the Palu IV Bridge, a type of steel arch bridge with hangers of 250 m and a width of 7.5 m. According to Mulchandani et al (2019) [1], the Palu IV bridge failed due to earthquake shocks accompanied by liquefaction events. Due to the multiplier effect, the horizontal displacement of the superstructure towards the transverse direction of the bridge is 5.50 m on the pier and 2.00 m on the abutment (see Figures 1 and 2). In addition, the failure of the Palu IV Bridge has also been simulated by Ghulam et al (2021) [2] with the result that the Arch structural element collapses. Another researcher, Imran et al (2019) [3], concluded that the Palu IV Bridge failed in the anchorage system of the bridge bearing due to the near-fault effect, which increased ground motion significantly. This confirms that the large displacement that appears can no longer be supported either by the support or by the superstructure, so the bridge collapsed.

One documented history of liquefaction events worldwide is the Niigata Earthquake in 1964, which caused the Showa Bridge to collapse (see Figure 3). According to Iwasaki (1984) [4]

[1*]Corresponding email: ahmad.rifai@ugm.ac.id
DOI: https://doi.org/10.20885/icsbe.vol4.art35

The Showa Bridge is one of the infrastructures that collapsed during an earthquake in Niigata City. Another researcher, Dash et al (2010) [5], stated that the Showa Bridge collapsed due to lateral loads and additional free-standing piles when the top soil layer experienced liquified, creating a large moment so that the piles on the pier experienced buckling failure. In addition, based on research by Bhattacharya and Madabhushi (2008) [6], Showa Bridge uses pinned and roller-type supports. The roller support during an earthquake is very susceptible to displacement, and when the displacement exceeds the permissible, the bridge collapses. According to Bhattacharya et al (2008) [7] A structure failure can occur with four mechanisms; shear failure, bending failure, Buckling, and dynamic amplification. The liquefaction phenomenon causes the length of fixity pile to increase in the liquefied soil layer. As a result, the structure can fail with the dynamic amplification mechanism. The results of the report by Yoshida et al (2007) [8] showed that The failure of the Showa bridge occurs due to increased displacement of the ground in circumstances where pile deformation occurred due to liquefaction. Therefore, infrastructure development in areas prone to earthquakes and liquefaction must strengthen the foundation to be safe.

After the Palu Earthquake, the Government of Indonesia, through Directorate General of Highways (DJBM), Ministry of Public Works and Public Housing (PUPR), issued Guidelines number: 02/M/BM/2021 concerning Practical Guidelines for Bridge Technical Planning 2021, which requires that each design of standard bridge in Indonesia with consideration the potential for liquefaction and its impact on bridges [9]. In the same year, DJBM issued Interim Special Specification number: Skh-1.7.47 concerning Earthquake Insulators using Lead Core Rubber Bearings for Bridges [10]. The use of Lead Rubber Bearing is intended to reduce earthquake forces and extend the natural period of the building structure at the same time.

Figure 1. Palu IV Bridge has collapsed after Palu Earthquake 2018 (Nurdin, 2021) [11].

Figure 2. Bridge support failed due to earthquake (Budiharto, 2021) [12].

Figure 3. Showa Bridge failure due to 1964 Niigata earthquake and liquefaction phenomenon (Kerciku et al 2008) [13].

The use of seismic isolators as earthquake force dampers in Indonesia is getting started to be applied in bridges because the location of Indonesia's territory is in a sizeable earthquake-prone zone. Based on the Indonesian Earthquake Source and Hazard Map published in 2017 by the National Earthquake Study Center (PUSGEN) of the Ministry of PUPR, almost all main island areas in Indonesia are prone to major earthquakes, except for Borneo Island, which has a lower category (see Figure 4).

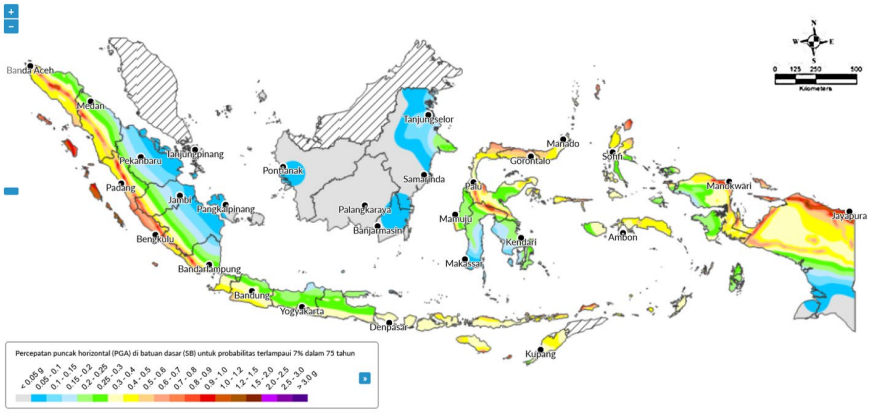

Figure 4. Indonesian earthquake map for 7% probability of exceedance in 75 years or equivalent to 1000 years period with modification [14].

2. BRIDGE RESEARCH LOCATION AND SPECIFICATION

2.1. Determination of PGA Value

This research is located in Kretek District, Bantul Regency, Yogyakarta Special Region Province, and the distance from the coast is <1 km. The location of the bridge is in a high-moderate liquefaction vulnerability zone according to the Atlas of Liquefaction Vulnerability Zones by Geology Agency (2019) [15], and it is near the Opak Fault (<10 km) [16]. This condition requires that each infrastructure built in this area consider the earthquake forces and liquefaction. According to Towhata (2008) [17], Liquefaction mitigation measures can be applied first by increasing the structural strength or reducing the seismic force. If this step is difficult to carry out, it is necessary to improve the soil with various methods that can reduce the intensity and potential for liquefaction events. For the last step, if there is no soil improvement, large deformations will emerge on the structure.

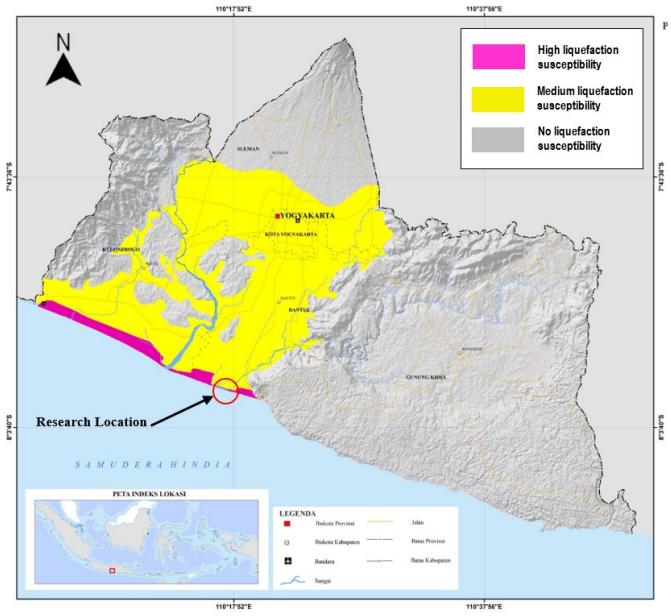

Figure 5. Liquefaction susceptibility zone map on Special region of Yogyakarta [15].

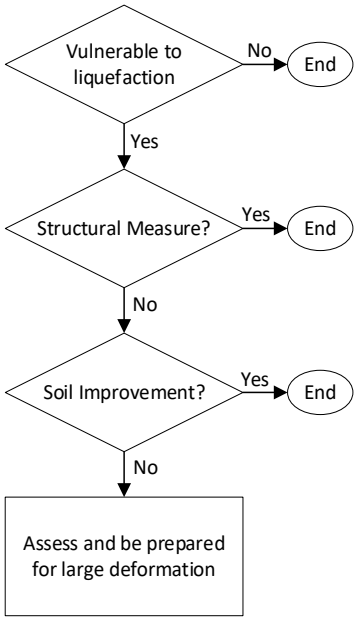

Figure 6. Flow of liquefaction mitigation (Towhata, 2008) [17].

2.2. Bridge specification

This study tried to compare the use of bearing support on the Kretek 2 Bridge. The Kretek 2 bridge uses a PCI Girder with a length of 40.8 m totaling eight spans (P1-P2-P3-P4-P5-P6-P7-P8-A2) with a total length of 343 m. An example of a Kretek 2 Bridge structure model on a pier can be seen in Figure 7 below. The girder load is transferred to the pier head through the bearing, then from the pier head, the load is transferred to the pier and finally supported by the pile cap.

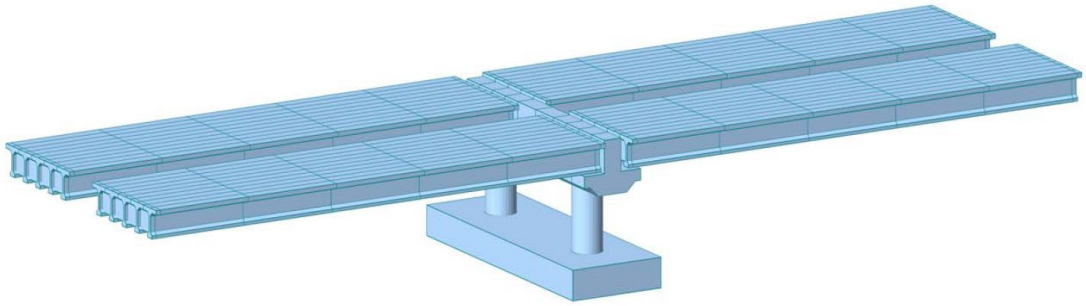

Figure 7. Bridge structure model (girder-pier head-pier-pile cap)

2.3. Bearing support

The bearings used as a load distributor adjust the structural system chosen. In Indonesia, the bearings used on bridges vary, including Pinned-Pinned Systems, Pinned-Rollers, Elastomeric Bearing Pads, and Lead Rubber Bearings. The most common use of bearings for PCI Girder bridges is an elastomeric bearing pad (or 'bearing pad'). But nowadays, lead rubber bearings are being promoted, including one at the Kretek Bridge 2. This study tries to compare the use of different bridge bearings using three types of systems: Pinned and Roller, Bearing Pad, and Lead Rubber Bearing. Although the pinned and roller

system is not commonly used in PCI Girder, the analysis results can be used as a benchmark against other bearing systems.
The bearing Pad is a rubber bearing covered with several steel plates inside. The use of bearing pads is regulated in SNI 3967:2008 concerning Specifications for plain type and layered elastomeric bearings for bridge support [18]. The elastomeric bearing design uses guidelines for bridge support from the Ministry of PUPR (2015). Displacement in bearing pads is limited to less than 50mm [19].

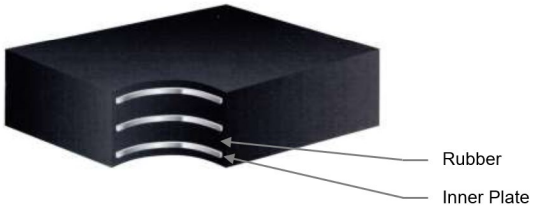

Figure 8. Elastomeric bearing pad (Magdatama, 2021) [20]

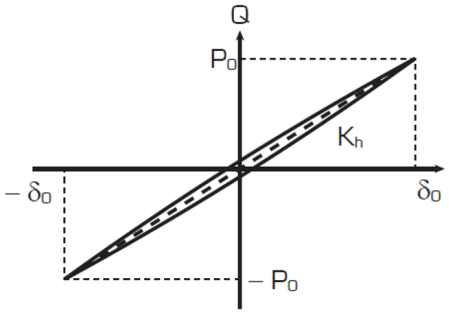

δ_0 = d : Displacement
P_0 : Maximum Load
K_h : Shear stiffness

Figure 9. A hysteresis loop of natural bearing (Bridgestone, 2015) [21]

Lead rubber bearing (LRB) is a base insulator with a larger damping ratio than bearing pads. The damping ratio is the amount of absorption of horizontal loads that can be accepted on a material or damping system. The following formula can calculate the damping ratio:

$$\xi = \frac{C}{2\,m\,\omega} \tag{1}$$

$$\omega = \frac{2\pi}{T} \tag{2}$$

$$T = 2\,\pi\sqrt{\frac{m}{\Sigma \quad K}} \tag{3}$$

where ξ is damping ratio (%), C is damping coefficient (kN.s/m), ω is angular frequency (rad/sec), T is time period, and K is stiffness. The main difference between lead rubber bearings and bearing pads is that lead is used as a core system which can provide a high initial characteristic strength. In addition, the thickness of the rubber layer, which is thicker than the bearing pad accompanied by an anchor and plate system, allows for large displacements (see Figures 10 and 11).

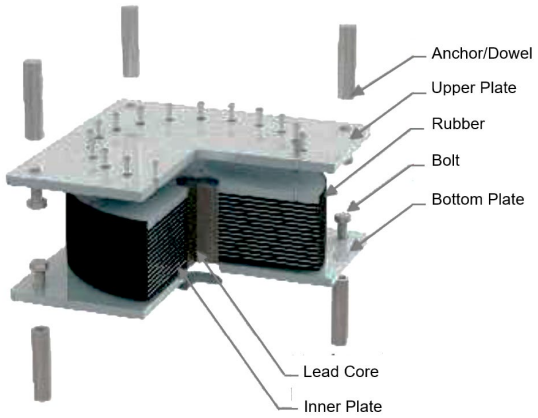

Figure 10. Lead rubber bearing (Magdatama, 2021) [22].

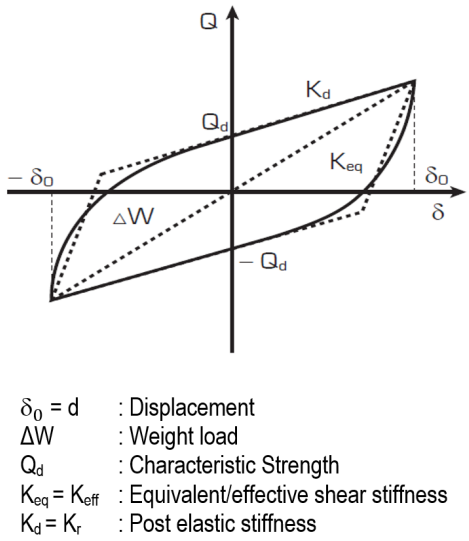

Figure 11. A hysteresis loop of lead rubber bearing (Bridgestone, 2015) [21].

Research on base insulators to reduce earthquake loads has been carried out by Islam et al (2015) [23], with the results that the base insulator can reduce shear forces and moments in buildings up to 50% and 45%, respectively. Another researcher Zulkifli (2018) [24], mentioned that modeling a box girder bridge structure using LRB can reduce shear forces and moments by up to 41%. In addition, Setiawan (2022) [25] stated that the use of LRB in the structure could reduce earthquake forces by up to 70% due to the extension of the period of the structure and coupled with the reduction of the increasing value of the damping ratio. Meanwhile, Delitriana (2022) [26] states that the use of LRB is suitable for long-span bridges with specifications of short piers, pile caps embedded in the ground, and short structural periods.

3. BRIDGE MODELLING IN MIDAS CIVIL

MIDAS Civil utilized research in the bearings has previously been carried out by Ginting (2019) [27] in examining the effectiveness of LRB on continuous span concrete bridges with the results of effective LRB performance on structures with high piers, increasing the period of the structure, and providing comfort performance even when large displacement on the superstructure of the bridge occurred compared to conventional bearings. Another researcher, Indra et al (2016) [28], concluded that the dynamic response analysis of the use of LRB on Steel Frame Bridges with the results of increasing LRB stiffness could increase the dynamic response of displacement as an energy dissipation process of earthquake loads. The application of Midas on a two-hinged arch suspended-deck bridge has also been carried out by Suryadi et al (2020) [29] on the Kalikuto Bridge; using LRB, the horizontal shear force is significantly reduced because the shear force can be transferred to each support evenly and then the energy dissipation mechanism occurs.

3.1. Input model

The model is carried out to determine the movement at the Bridge Pier. Due to the span length and uniform load, the bridge model can be simplified according to the dimensions of the Pier P5 structure, which has a maximum pier height of 5.5 m. The model uses 2 spans with 4 supports; The 2 supports are modeled completely with Pier Head, Pier, and

Pile Cap, while the other 2 supports are modeled directly as supports (see Figure 12). The force and displacement maximum values are intended to emerge at the Pier position. With the same model structure, proceed with creating 3 models based on the type of support being reviewed; 1) Pinned and Roller, 2) Bearing Pad, and 3) Lead Rubber Bearing.

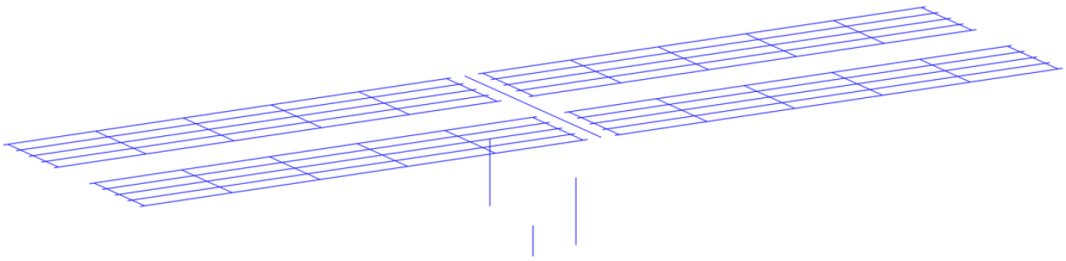

Figure 12. Bridge modelling in MIDAS Civil

3.2. Input bearing specification

Each model requires input data in accordance with the type of placement used. Pinned and Roller can be modeled by defining Pinned support and Roller support so that on the pedestal on the Pier Head under review there are two different types of support. The bearing pad support model can be modeled by defining it as an Elastic Link with different inputs on the x, y, and z axes correlating to the value of spring stiffness. According to Akogul and Celik (2008) [30], the stiffness value can be calculated by the following formula:

$$K_h = K_{eff} = \frac{G\,A}{t_e} \tag{4}$$

$$K_v = \frac{E_c\,A}{t} \tag{5}$$

$$K_\theta = \frac{E\,I}{t_e} \tag{6}$$

$$E_c = 4.8\,G\,{S_f}^2 \tag{7}$$

$$S_f = \frac{L'\,W}{2h_{ri}(L'\,W)} \tag{8}$$

where K_h is lateral stiffness, K_v is vertical stiffness, K_θ is rotational stiffness, G is shear modulus, E_c is elasticity modulus, A is bearing cross-sectional area, I is inertia of the shape of the bearing, t is total thick of bearing, t_e is total rubber layer thick of bearing, S_f is shape factor, L^' is length dimension of bearing, W is width dimension of bearing, and h_ri is thick of bearing. K_v is input as spring stiffness with notation 〖SD〗_(x), K_h value is input as spring stiffness with notation 〖SD〗_(y), 〖SD〗_(z), and K_θ for rotational spring stiffness notation 〖RD〗_(x), 〖RD〗_(y), 〖RD〗_(z) with X, Y and Z directions, respectively. The specifications for the bearing pad used in the modeling and generally also used in PCI Girder spans of 40.8 m can be seen in Table 1 below:

ISSN 2541-223X
Volume 4 2022

Table 1. Bearing pad specification

Specification	Detail	Unit
Dimension (L'·W·t)	450·400·60	mm
Hardness	50	duro
Shear Modulus, G	0.60	MPa
Rubber yield strength, f_{yr}	15.5	MPa
Plate yield strength, f_{ys}	240	MPa
N layer of plate	5	layer
Cover thick	0.55	mm
Layer thick	0.85	mm
Plate thick	0.30	mm

Meanwhile, LRB modeling is defined as a General Link type Lead Rubber Bearing Isolator. This study is also intended to assess the ability of the LRB unit that has been installed on the Kretek 2 Bridge with specifications that have gone through the results of laboratory tests which can be seen in Table 2. While to determine the energy dissipated per cycle, W_d can be calculated [31] with the following formula:

$$W_d = 2\,\pi\,K_{eff}\,D^2\,\xi_{eff} \quad (9)$$

$$Q_d = \frac{W_d}{4D} \quad (10)$$

$$K_d = K_{eff} - \frac{Q_d}{D} \quad (11)$$

$$r = \frac{D}{V - Q_d} \quad (12)$$

where D is maximum displacement, ξ_{eff} is effective damping ratio (%), Q_d is characteristic strength, K_d is post-yield stiffness, r is post yield ratio, and V is vertical load. The LRB Input Properties in Midas are divided into 2 parts; 1) Linear property section by entering the effective stiffness value, K_{eff} and effective coefficient damping, C with the notation D_x, D_y, D_z, and 2) the Nonlinear Properties section by entering a value K_d, r, and rubber yield strength, f_{yr} with the notation D_x, D_y, D_z.

Table 2. Lead rubber bearing specification

Specification	Detail	Unit
Type	LRB-N D700·189	
Rubber diameter	700	mm
Total height	933	mm
Rubber height	313	mm
Plate dimension	750·750	mm
Rubber yield strength, f_{yr}	15.5	MPa
Horizontal stiffness effective, K_{eff}	2.29	kN/m
		m
Vertical load, V_{bd}	2600	kN
Seismic vertical load, V_{Ed}	1300	kN
Effective damping at d_{bd}	25.21	%

Displacement ultimit load, d_{bd}	252	mm
Displacement earthquake load, d_{Ed}	384	mm

4. BRIDGE LOADS

Bridge loading refers to SNI 1725:2016 [32], which divides the load into permanent and transient loads. Calculating the permanent load is generally based on the volume of structure's shape multiplied by the material's unit weight. The unit weight and mass density used as a reference are as follows:

Table 3. Weight and mass density material

Material	Weight (kN/m^3)	Mass density (kg/m^3)
Compacted sand, silt or clay	17.2	1755
Rolled gravel, macadam or ballast	18.8-22.7	1920-2315
Asphalt concrete	22.0	2245
Lightweight concrete	12.25-19.6	1250-2000
Concrete f'$_C$<35 MPa	22.0-25.0	2320
Concrete 35 < f'$_C$<105 MPa	22 + 0.022 f'$_C$	2240 + 2.29 f'$_C$
Steel	78.5	7850

4.1. Load combinations

In the regulation of SNI 1725:2016, the combination of loads in the section becomes an ultimate combination to determine the ultimate limit, a service combination to determine the service limit, an extreme combination to determine the extreme limit of the condition or ship collision, flooding or other hydraulic loads, and a fatigue combination to determine the limit fatigue from a load of repetitions. In this study, knowing the bearing performance during an earthquake is limited by using a combination of extreme earthquake conditions with the following formula:

$$(\ _{MS}M_S + \ _{MA}M_A + \ _{PR}P_R) + \ _{EQ}(T_T + T_D + T_B + T_P) + E_Q \quad (13)$$

where M_S, M_A, and P_R are permanent loads for dead load, additional dead load, and prestressed load, respectively, whereas T_T, T_D, T_B, T_P, and E_Q are transient loads for trucks, lane loads, brake loads, pedestrian loads, and earthquake loads, respectively. Meanwhile, is load factor that adjusted to the condition of the bridge structure.

In this study, Permanent loads consist of M_S for dead weight of the structure, M_A for parapet, median, asphalt concrete, and rainwater loads, and P_R for prestressed loads in PCI Girder. The dead load factor, $_{MS}$ is used 1.3 because the dominant structure is cast in place, for additional dead load factor, $_{MA}$ is used 2.0 for the usual ultimate limit state, and the prestressed load factor $_{PR}$ is used 1.0. Transient load factor during an earthquake, $_{EQ}$ used 0.5 because the bridge is very important classification. The transient loads for truck loads, lane loads, and brake loads also follow the provisions of SNI 1725:2016.

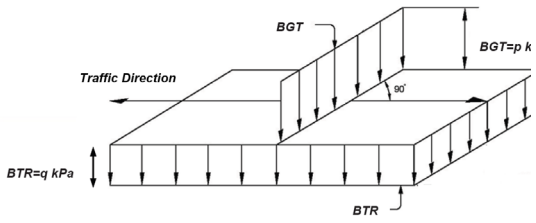

Figure 13. Lane Load "D" [32]

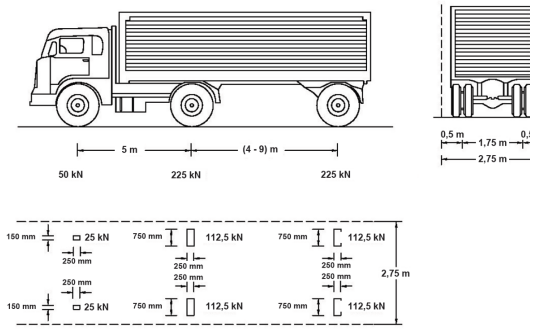

Figure 14. Truck Load "T" [32]

4.2. Earthquake loads

The bridge location that is close to the source of the opaque fault (<10 km) requires that the earthquake load use site-specific response analysis, and it is not allowed to use the response spectrum contained in SNI 2833:2016 concerning Bridge Planning Against Earthquake Loads [33]. The earthquake load used is based on research by Asrurifak (2021) [23], who has calculated the site-specific response spectra (SRSS) based on the seven ground motions of the following significant earthquakes; 1) 1995 Kobe Japan, 2) 2000 Tottori Japan, 3) 2010 Darfield New Zealand, 4) 1979 Imperial Valley USA, 5) 1987 Superstition Hills USA, 6) 1992 Erzincan Turkey, 7) 1989 Loma Prieta USA which has been spectra matching and scaling of the amplification into a response spectrum at ground level (see Figure 15). The result is that the SRSS value is higher than all response spectra using SNI 2833:2016, which uses a 7% probability of exceedance in 75 years or equivalent to 1000 years period. Based on the direction of the earthquake on the structure, the earthquake load is divided into x direction, E_{Qx}, and y direction, E_{Qy}, then the combination of earthquake loads used are; Extreme1 $(E_{Qx} + 0.5\,E_{Qy})$, Extreme2 $(E_{Qx} - 0.5\,E_{Qy})$, Extreme3 $(0{,}5\,E_{Qx} + E_{Qy})$, and Extreme4 $(-0.5\,E_{Qx} + E_{Qy})$.

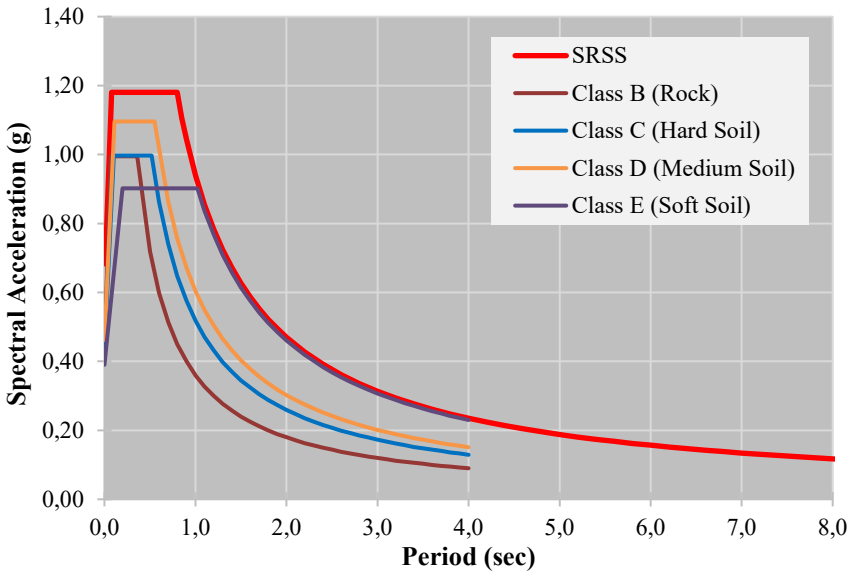

Figure 15. Response spectrum design (SRSS and SNI 2833-2016)

5. RESULT AND DISCUSSION

After modeling and all finished loads are inputted into MIDAS Civil, a running program is carried out with 3 models, pinned and roller, bearing pad, and lead rubber bearing, to analyze the internal forces acting on the bridge structure. The analysis results are beam force and displacement outputs for each combination of Extreme1, Extreme2, Extreme3, and Extreme4.

5.1. Beam force output

The internal force output includes axial force, z-direction shear, y-direction shear, z-direction moment, and y-direction moment. The output results for the LRB placement model can be seen in Figures 16 to 20. The overall results for each model are summarized in the form of Tables 4 to 6.

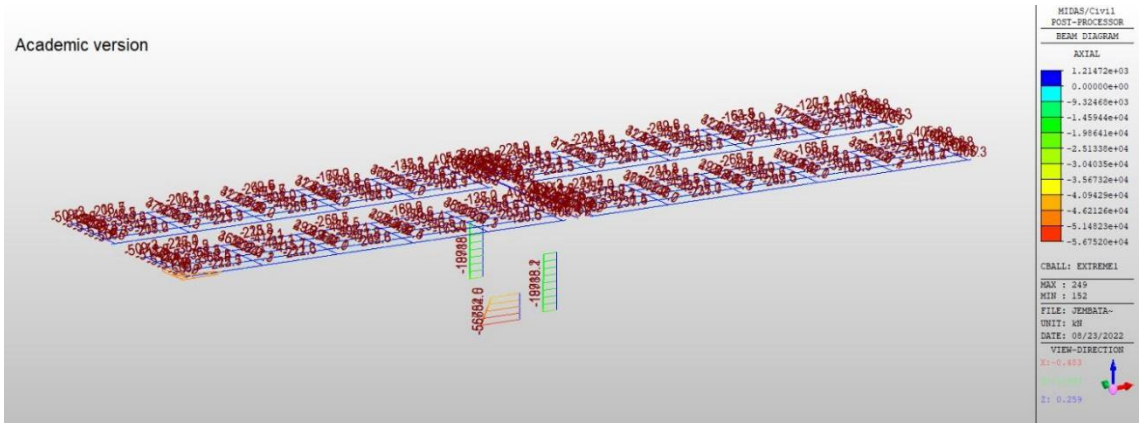

Figure 16. Extreme1 condition axial force on bridge with LRB support

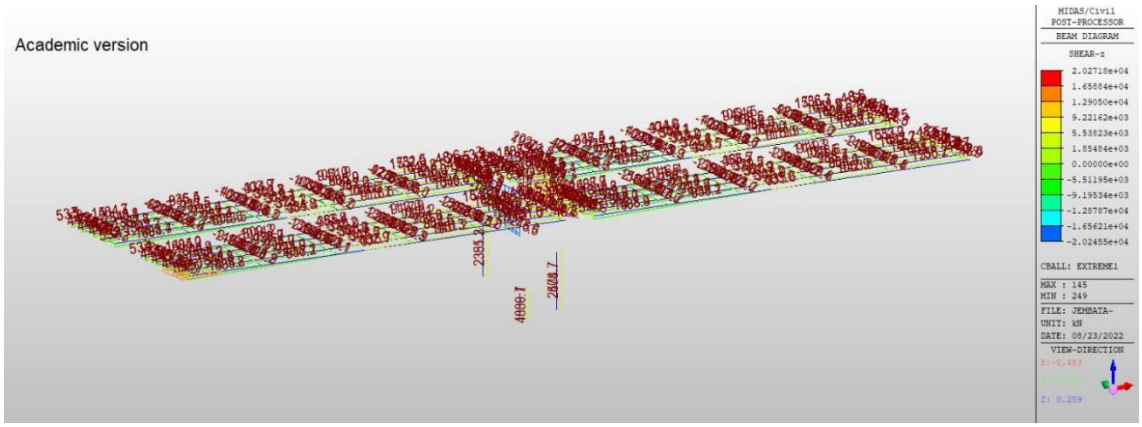

Figure 17. Extreme1 condition shear z force on bridge with LRB support.

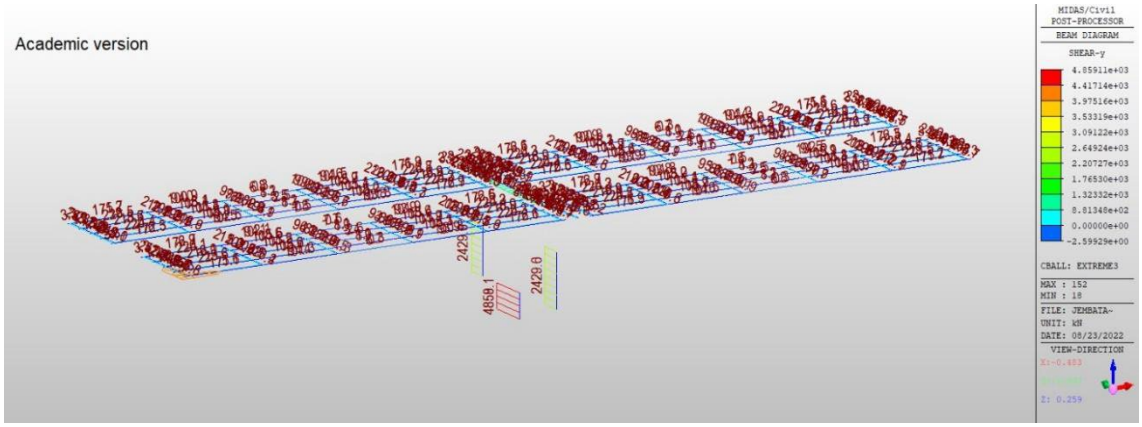

Figure 18. Extreme1 condition shear y force on bridge with LRB support.

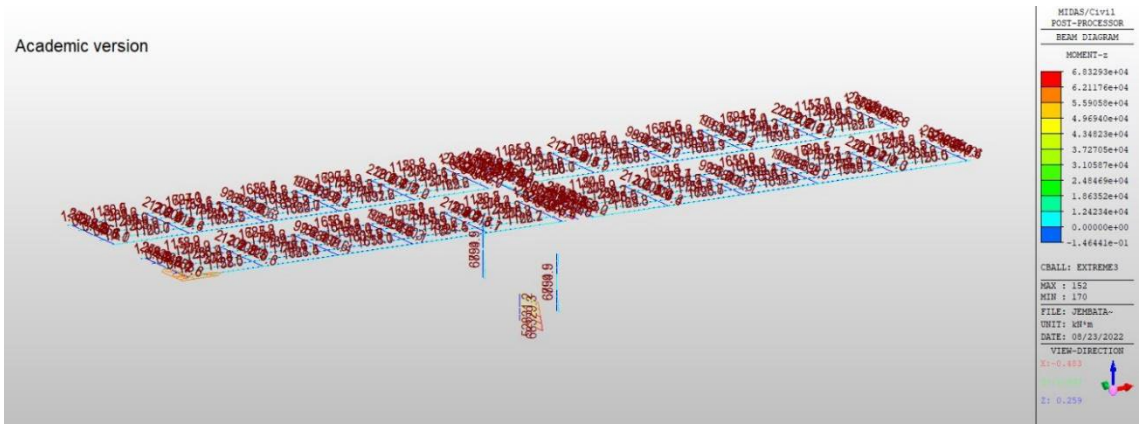

Figure 19. Extreme1 condition moment z force on bridge with LRB support.

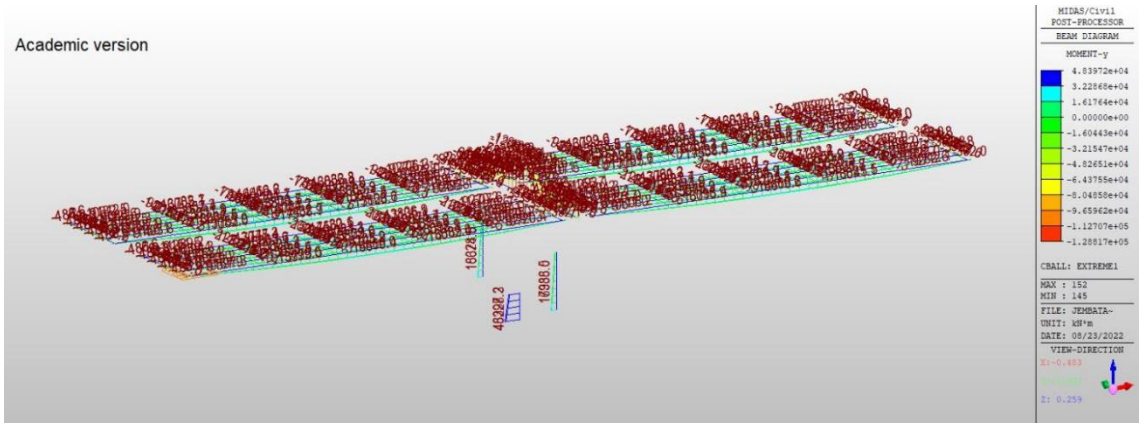

Figure 20. Extreme1 condition moment y force on bridge with LRB support.

Table 4. Beam force output from pinned and roller support model.

Load Combinations	Axial (kN)	Shear Y (kN)	Shear Z (kN)	Moment Y (kN*m)	Moment Z (kN*m)
Extreme1	-59488.29	2434.90	-3661.25	80464.37	40903.60
Extreme2	-59488.29	-2414.09	-3661.25	80464.37	-41053.45
Extreme3	-60885.33	4615.18	-5438.32	68436.60	67542.25
Extreme4	-63679.41	4615.18	-8992.48	44381.04	67542.25

ISSN 2541-223X
Volume 4 2022

Table 5. Beam force output from bearing pad support model

Load Combinations	Axial (kN)	Shear Y (kN)	Shear Z (kN)	Moment Y (kN*m)	Moment Z (kN*m)
Extreme1	-56553.12	2284.61	4633.15	45642.05	33017.06
Extreme2	-56588.12	-2238.24	4623.36	45524.98	-38841.41
Extreme3	-56626.31	4539.62	2344.56	23601.90	60968.78
Extreme4	-56807.69	4528.14	-2284.62	-23765.43	60699.90

Table 6. Beam force output from lead rubber bearing support model

Load Combinations	Axial (kN)	Shear Y (kN)	Shear Z (kN)	Moment Y (kN*m)	Moment Z (kN*m)
Extreme1	-56752.00	2429.82	4880.75	48397.15	38039.19
Extreme2	-56752.00	-2429.82	4880.75	48397.15	-38039.19
Extreme3	-56752.00	4859.11	2450.79	24990.78	68329.34
Extreme4	-56752.00	4859.11	-2450.79	-24990.78	68329.34

The results of the analysis show that in the pinned and roller model, the most considerable axial load occurs at Extreme4 with a value of 63679.41 kN, the most considerable shear Y at Extreme3 and 4 with a value of 4615.18 kN, the most considerable shear Z at Extreme4 with a value of 8992.48 kN, the largest moment Y is at Extremes1 and 2 with a value of 80464.37 kN, and the most considerable moment Z are at Extreme3 and 4 with a value of 67542.25 kN. The use of pinned and roller causes the dominant shear force to occur in the Z direction. In the bearing model, the most considerable axial load occurs at Extreme4 with a value of 56807.69 kN, the most considerable shear Y at Extreme3 and 4 with a value of 4539.62 kN, the most considerable shear Z at Extreme1 and 2 with a value of 4633.15 kN, the most considerable moment Y at Extreme1 with a value of 45642.05 kN, and the most considerable moment Z at Extreme3 with a value of 60968.78 kN. The bearing pad used shows that shear forces are more evenly distributed in the Y and Z directions. While in the LRB model, there is an even distribution of axial loads in all Extreme combinations with a value of 56752.00 kN, the most considerable shear Y at Extremes3 and 4 with a value of 4859.11 kN, the most considerable shear Z at Extreme1 and 3 with a value of 4880.75 kN, the most considerable moment Y at Extreme1 and 2 with a value of 48397.15 kN, and the most considerable moment Z at Extreme3 and 4 with a value of 68329.34 kN. The use of LRB shows the existence of damping as a dissipation of earthquake energy so that the axial force is the same even though there is a difference in the direction of the earthquake. Consistency also occurs in shear and moment forces; the values at Extremes1 and 2 show similarity, as well as for Extremes3 and 4. The following graph presents the recapitulation values of the three models' output forces:

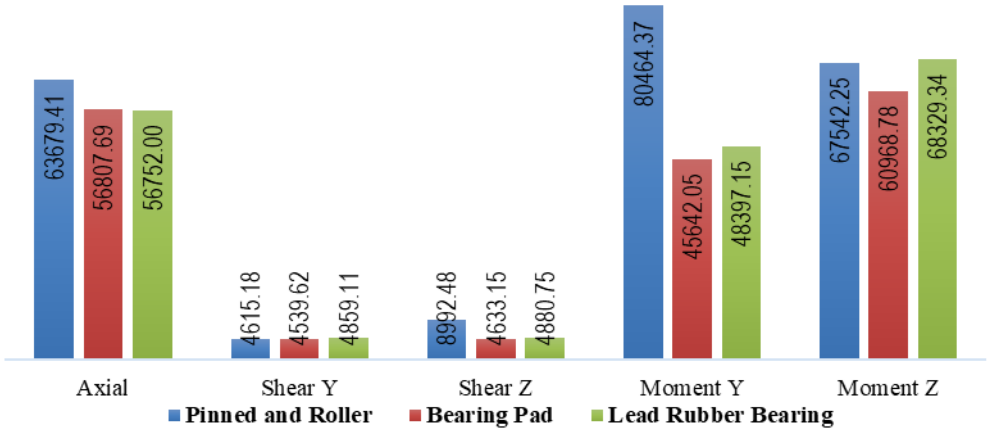

Figure 21. Beam force at pile cap bottom.

The bearing pad and lead rubber bearing models exhibit significantly reduced beam forces compared to the pinned and roller models. The bearing pad and lead rubber bearing decreased by -10.79% and -10.88% for the axial force, respectively. For the shear Y force, there was a decrease in the bearing pad up to -7.28% and an increase in lead rubber bearing up to 5.29%. For the shear Z force, the bearing pad and lead rubber bearing decreased by -74.59% and -72.75%, respectively. The bearing pad and lead rubber bearing were reduced by -65.51% and -63.48% for the moment Y, respectively. For moment Z force, there was a decrease in the bearing pad and lead rubber bearing up to -19.28% and -7.34%, respectively. The result using the bearing pad and lead rubber bearing dominantly reduces the shear force in the Z direction and the moment in the Y direction significantly so that the earthquake forces can be evenly distributed in each direction.

Table 7. Presentation comparison beam force output.

Load Combi-nations	Pinned and Roller Vs. Bearing Pad					Pinned and Roller Vs. Lead Rubber Bearing				
	Axial (%)	S_Y (%)	S_Z (%)	M_Y (%)	M_Z (%)	Axial (%)	S_Y (%)	S_Z (%)	M_Y (%)	M_Z (%)
Extreme 1	-4.93	-6.17	26.55	-43.28	-19.28	-4.60	-0.21	33.31	-39.85	-7.00
Extreme 2	-4.88	-7.28	26.28	-43.42	-5.39	-4.60	0.65	33.31	-39.85	-7.34
Extreme 3	-7.00	-1.64	-56.89	-65.51	-9.73	-6.79	5.29	-54.93	-63.48	1.17
Extreme 4	-10.79	-1.89	-74.59	-46.45	-10.13	-10.88	5.29	-72.75	-43.69	1.17

5.2. Displacement output

In addition to knowing the value of the beam forces, it is also essential to know the displacement behavior that occurs in the three models. Theoretically, a large earthquake force triggers a large lateral force, the impact of which is an enlargement of the horizontal shift in the structure of the bridge. If the shift that occurs exceeds the ability of a bearing to withstand these forces, the superstructure can be separated from its position, and eventually, collapse occurs.

ISSN 2541-223X
Volume 4 2022

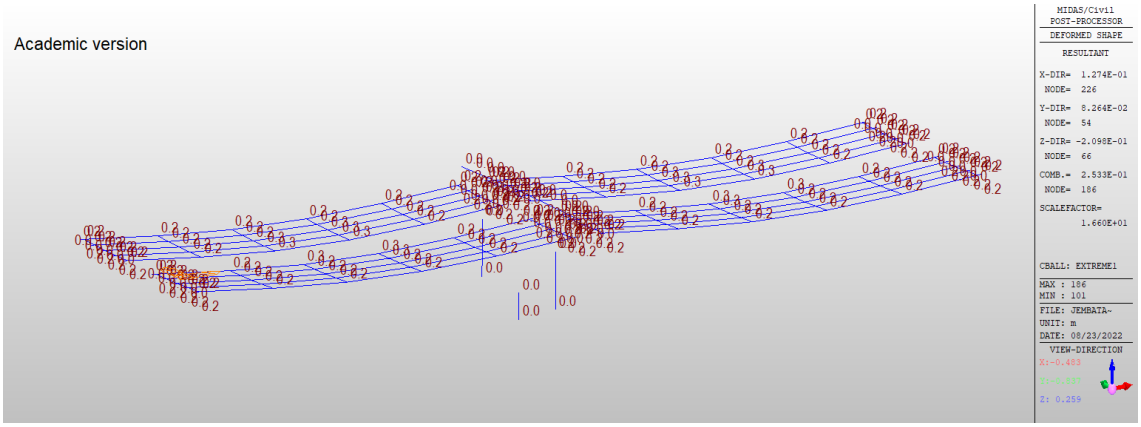

Figure 22. Extreme1 condition for displacement on bridge with LRB support.

Table 8. Displacement output

Load Combinations	Pinned and Roller		Bearing Pad		Lead Rubber Bearing	
	D_Y (m)	D_Z (m)	D_Y (m)	D_Z (m)	D_Y (m)	D_Z (m)
Extreme1	0.0745	0.0613	0.1204	-0.1832	0.0672	-0.1387
Extreme2	-0.0755	-0.0582	-0.1093	-0.2214	-0.0662	-0.1624
Extreme3	0.1480	0.0851	0.1935	-0.1646	0.1270	-0.1385
Extreme4	0.1480	0.0849	0.1892	-0.1657	0.1266	-0.1387

The displacement occurs in the pinned and roller up to 0.148m and 0.0851m for the Y and Z directions, respectively. On the bearing pad, the most significant displacement occurs up to 0.1935m for the Y direction and 0.2214m for the Z direction. While in the LRB, there is a displacement of up to 0.1270m and 0.1624m for the Y and Z directions, respectively. The displacement value on the bearing pad exceeds the permit requirement of 0.050m [19], so even though the stiffness value of the bearing pad can absorb earthquakes, it is limited. The location of the bridge structure close to the earthquake source, such as the Kretek 2 Bridge, will also produce a considerable displacement value. Because of that, we need an LRB with an extensive damping capability and can accommodate a large displacement.

Table 9. Allowable displacement for bearing

	Direction	Displacement Maximum (mm)	Displacement Allowable (mm)	Result
Bearing Pad	Y	0.1935	0.050	Not Ok
450·400·60	Z	0.2214	0.050	Not Ok
Lead Rubber Bearing	Y	0.1270	0.384*	Ok
LRB-N D700·189	Z	0.1624	0.384*	Ok

*Displacement from laboratory test when earthquake occurred.

6. CONCLUSION

The Kretek 2 Bridge is prone to significant earthquakes and liquefaction due to the Opak fault nearby. Bridge modeling use 3 types of bearings, pinned and roller, bearing pad, and lead rubber bearing to calculate beam forces and displacements. The bridge loading refers to SNI 1725:2016, and the response spectra used use site-specific response results based on SNI 2833:2016. The MIDAS Civil analysis shows that both bearing pad and lead rubber bearing significantly reduce beam force compared to the pinned and roller models. The bearing pad decreases against axial force by -10.79%, Y shear force by -7.28%, Z shear force by -74.59%, Y moment force by -65.51%, and moment Z force by - 19.28%. Meanwhile, lead rubber bearings also decreased axial forces by -10.88%, Y shear forces by 5.29%, Z shear forces by -72.75%, Y moment forces by -63.48%, and Z moment forces by -7.34%. This shows that both the use of bearing pad and LRB dominantly reduce the shear force in the Z direction and the Y moment significantly so that the earthquake force can be evenly distributed in each direction. As for the displacement that occurs in the pinned and roller of 0.148m for the Y direction, the bearing pad is 0.221m for the Z direction, and on the LRB, it is 0.162m for the Z direction. Based on the displacement limit, the bearing pad is regarded to be no longer able to withstand the displacement that occurs. While in LRB, displacement of up to 0.384m can be permitted. The findings of this study show that using LRB to reduce seismic forces is appropriate for bridge constructions with small pier heights. Another option for future research is to use time history analysis as a nonlinear dynamic analysis to assess the performance of the LRB's hysteresis loop.

7. REFERENCES

Mulchandani H K Pilani S Robertson I N Prevatt D O and Roueche D, 2019 StEER : Structural Extreme Event Reconnaissance Network PALU EARTHQUAKE StEER : Structural Extreme Event Reconnaissance Network **1**, January.

Ghulam B R Desmaliana E and Widyaningsih E, 2021 Analisis Dinamik Jembatan Pelengkung (Studi Kasus : Jembatan Palu IV) *Reka Racana J. Online Inst. Teknol. Nas.* **xx**, x p. 1–14.

Imran I Santoso B Pramudito A and Zamad M K, 2019 *Simulation of Palu IV Bridge Collapse using near-fault ground motions* .

Iwasaki T, 1984 A Case History of Bridge Performance During Earthquakes in Japan A Case History of Bridge Performance During Earthquakes in Japan May.

Dash S R Bhattacharya S and Blakeborough A, 2010 Bending-buckling interaction as a failure mechanism of piles in liquefiable soils *Soil Dyn. Earthq. Eng.* **30**, 1–2 p. 32–39.

Bhattacharya S and Madabhushi S P G, 2008 A critical review of methods for pile design in seismically liquefiable soils *Bull. Earthq. Eng.* **6**, 3 p. 407–446.

Bhattacharya S Dash S R and Adhikari S, 2008 On the mechanics of failure of pile-supported structures in liquefiable deposits during earthquakes *Curr. Sci.* 94, 5 p. 605–611.

Yoshida N *et al.*, 2007 Causes of showa bridge collapse in the 1964 niigata earthquake based on eyewitness testimony *Soils Found.* 47, 6 p. 1075–1087.

Direktorat Jenderal Bina Marga, 2021 *Panduan Praktis Perencanaan Teknis Jembatan* 02/M/BM/20 Jakarta: Direktorat Jenderal Bina Marga.

Direktorat Jenderal Bina Marga, 2021 *Isolator Gempa Menggunakan Bantalan Karet Inti Timbal (Lead Rubber Bearing) untuk Jembatan* SKh-1.7.47 Jakarta: Kementerian Pekerjaan Umum dan Perumahan Rakyat.

Nurdin S, 2021, Study Forensic Terhadap Kerusakan Struktur Akibat Likuifaksi Pada Gempa Palu 2018 di Sulawesi Tengah, Palu.

Budiharto P, 2021, Evaluasi Kinerja Struktur Jembatan Beruji Kabel Pasupati Bandung Berdasarkan Peraturan SNI 1725:2016 dan SNI 2833:2016 serta Analisis Nonlinier Pushover, Institut Teknologi Bandung.

Kerciku A A Bhattacharya S Lubkowski Z A and Burd H J, 2008 Failure of Showa Bridge During the 1964 Niigata Earthquake: Lateral Spreading or Buckling Instability? *14 th World Conf. Earthq. Eng.* October 2014 p. 8.

Pusat Studi Gempa Nasional, 2017 *Peta Sumber dan Bahaya Gempa Indonesia Tahun 2017* Jakarta: Kementerian Pekerjaan Umum dan Perumahan Rakyat.

Badan Geologi, 2019 *Atlas Zona Kerentanan Likuefaksi Indonesia* Bandung: Kementerian Energi Sumber Daya Mineral.

Sari E K, 2017, Perancangan Fondasi Tiang Bor pada Jembatan Kretek 2 Bantul, Yogyakarta, Universitas Gadjah Mada.

Towhata I Wu W and Borja R I, 2008 *Geotechnical Earthquake Engineering* 1 .

Badan Standardisasi Nasional, 2008 *SNI 3967- 2008 : Spesifikasi bantalan elastomer tipe polos dan tipe berlapis untuk perletakan jembatan* 3967th ed. Jakarta.

Kementerian Pekerjaan Umum dan Perumahan Rakyat, 2015 *Pedoman Perancangan Bantalan Elastomer untuk Perletakan Jembatan* 10/SE/M/20 Jakarta: Kementerian Pekerjaan Umum dan Perumahan Rakyat.

Magdatama, 2021 *Magda Elastomer Bearing* Jakarta: PT Magdatama Multi Usaha.

Bridgestone, 2015 *Seismic Isolation Product Line-up* Version 20, 1 Tokyo: Bridgestone Engineered Products of Asia Sdn Bhd.

Magdatama, 2021 *Magda LRB* **2** Jakarta: PT Magdatama Multi Usaha.

Saiful Islam A B M Jumaat M Z Hussain R R Hosen M A and Huda M N, 2015 Incorporation preference for rubber-steel bearing isolation in retrofitting existing multi storied building *Comput. Concr.* 16, 4 p. 503–529.

Zulkifli E, 2018, Modul Kuliah SI-6112 Rekayasa Jembatan : Bridge Dynamics, Bandung.

Setiawan K, 2022, Mengenal Lead Rubber Bearing (LRB) Produksi Dalam Negeri, Jakarta.

Delitriana A, 2022, Effektivitas Penggunaan LRB pada Struktur Jembatan, Bandung.

Ginting T J, 2019, Studi Parametrik Efektifitas Lead Rubber Bearing (LRB) Pada Jembatan Beton Bentang Menerus, Institut Teknologi Bandung.

Indra A V Suryanita R and Ismeddiyanto, 2016 Analisis Respons Dinamik Jembatan Rangka Baja Menggunakan Sistem Seismic Isolation Lead Rubber Bearing (LRB) *Jom FTEKNIK* **3**, 1 p. 1–12.

Suryadi T Delitriana A Fukar Z and Tjendana R, 2020 Seismic isolation system of two hinged arch suspended-deck bridge: A case study on Kalikuto bridge-Indonesia *E3S*

Web Conf. 156.

Akogul C and Celik O, 2008 Effect of Elastomeric Bearing Modeling Parameters on the Seismis Design of RC Highway Bridges with Precast Concrete Girders *14th World Conf.*

Amin A Islam M and Ahamed M J, 2020 Base isolation of multi-storied building using lead rubber bearing *ITEGAM- J. Eng. Technol. Ind. Appl.* 6, 26.

Badan Standardisasi Nasional, 2016 *SNI 1725:2016 Pembebanan untuk Jembatan* 1725 .

Badan Standarisasi Nasional Indonesia, 2016 *SNI 2833:2016 Perencanaan Jembatan Terhadap Beban Gempa* 2833rd ed. Jakarta.